Journal of Advanced Ceramics
2017, **6**(4): 320–329
https://doi.org/10.1007/s40145-017-0244-2
ISSN 2226-4108
CN 10-1154/TQ

Research Article

ZrB_2–SiC based composites for thermal protection by reaction sintering of ZrO_2+B_4C+Si

R. V. KRISHNARAO*, V. V. BHANUPRASAD, G. MADHUSUDHAN REDDY

Defence Metallurgical Research Laboratory, Kanchanbagh, Hyderabad-500058, India

Received: June 20, 2017; Revised: August 23, 2017; Accepted: August 30, 2017

Abstract: Synthesis and sintering of ZrB_2–SiC based composites have been carried out in a single-step pressureless reaction sintering (PLRS) of ZrO_2, B_4C, and Si. Y_2O_3 and Al_2O_3 were used as sintering additives. The effect of ratios of ZrO_2/B_4C, ZrO_2/Si, and sintering additives (Y_2O_3 and Al_2O_3), was studied by sintering at different temperatures between 1500 and 1680 ℃ in argon atmosphere. ZrB_2, SiC, and YAG phases were identified in the sintered compacts. Density as high as 4.2 g/cm^3, micro hardness of 12.7 GPa, and flexural strength of 117.6 MPa were obtained for PLRS composites. Filler material was also prepared by PLRS for tungsten inert gas (TIG) welding of the ZrB_2–SiC based composites. The shear strength of the weld was 63.5 MPa. The PLRS ZrB_2–SiC composites exhibited: (i) resistance to oxidation and thermal shock upon exposure to plasma flame at 2700 ℃ for 600 s, (ii) thermal protection for Cf–SiC composites upon exposure to oxy-propane flame at 2300 ℃ for 600 s.

Keywords: ZrB_2; SiC; reactive sintering; synthesis; composites

1 Introduction

Zirconium diboride (ZrB_2) is well known for its unique combination and high values of properties: melting point, chemical stability, hardness, strength, thermal conductivity, and electrical conductivity. It is useful for extreme thermal and chemical environments existed in hypersonic flight, rocket propulsion, and atmospheric re-entry [1–3].

For the last decade, the research on synthesis and sintering of ZrB_2 based composites have been accelerated because ZrB_2 is being considered for high speed aircraft leading edges, and for structural parts in high temperature environments. The effect of different additives and open porosity on fracture toughness and thermal shock resistance of ZrB_2–SiC based composites prepared by spark plasma sintering (SPS) was reported [4,5]. Addition of carbon short fibers is shown to affect the densification and grain growth of ZrB_2–SiC based composites prepared by hot pressing (HP) [6,7]. Similarly, addition of AlN and nano-sized carbon black effects the densification and mechanical properties of HP ZrB_2–SiC based composites [8,9]. However, the high cost of ZrB_2 powders and difficulty in shaping large size components by SPS, HP, and fabrication by joining limit the usage of ZrB_2–SiC based composites.

Variety of synthesis routes which include: (i) reduction processes [10–12], (ii) chemical routes [13], and (iii) reactive processes [14] can be resorted to prepare ZrB_2 powders using ZrO_2 as a source of zirconium. The reduction route is relatively much cheaper than other routes for ZrB_2 synthesis. ZrO_2 can be reduced with B_2O_3+C, B_4C+C, or elemental boron. ZrC, C, and B are the typical impurities. ZrB_2 obtained

*Corresponding author.
E-mail: rvkr4534@yahoo.com

is agglomerated and requires extensive milling/pulverization to decrease the particle size to improve its sinter ability. But impurities from materials used for milling and oxygen from surface oxidation of particles introduced during pulverization deteriorate the densification behavior and properties of ceramics.

The reduction of ZrO_2 with B_4C was studied extensively [15]. Source of carbon and reaction atmosphere affect the synthesis temperature and morphology of ZrB_2 [16]. Yuan *et al.* [17] prepared porous ceramics of ZrB_2 by two-step sintering method, using spark plasma sintering–reactive synthesis. ZrB_2 porous ceramics were first synthesized using ZrO_2 and B_4C as precursors, and then sintered to ZrB_2 porous ceramics [18]. In our previous work, B_4C reduction of ZrO_2 to form impurity (ZrC, C)-free ZrB_2 was reported [19]. Further, composite powders of ZrB_2–SiC with particle sizes ranging from sub-micron to nanometer have been produced by rapid heating a mixture of ZrO_2+B_4C+Si, in an air furnace [19] and in air without using any furnace [20].

As mentioned above, ZrB_2 is being considered for high speed aircraft leading edges, and for structural parts in high temperature environments. The peak thermal stress of ultra high temperature ceramic (UHTC) wing leading edge (WLE) under re-entry heating conditions is predicted to be 80 MPa. It is well below the strength of pressureless sintered (PLS) UHTCs [21]. Heat resistant ceramic parts like ceramic aero-shell that protects spacecraft or hypersonic aircraft from heat, pressure, and debris are now 3D printable [22]. Ceramic foams are attractive for this application, but their poor mechanical properties make them unsuitable. 3D printed leading edge ceramic lattice structures are 10 times stronger than commercially available foams [23].

For thermal protection system (TPS) application, high mechanical performance is not required while oxidation resistance is the main material requirement. ZrB_2–SiC based multilayer materials are produced by tap casting and sintering without pressure assistance for aerospace applications. A three-level multifunctional TPS was developed with external part constituted by ceramic multilayer based on ZrB_2–SiC which in turn brazed to Cf–SiC composites and Si–SiC foams [24].

In our previous work, pressureless sintering (PLS) of ZrB_2–SiC–B_4C composites with Y_2O_3+Al_2O_3 addition has been reported [25]. The composites exhibited good dimensional stability and thermal shock resistance at 2200 ℃ in oxy-acetylene flame and at 2700 ℃ in plasma flame. In the present study, an attempt is made to synthesize and sinter ZrB_2–SiC based composites in a single-step PLRS using ZrO_2, B_4C, and Si for synthesis and Y_2O_3 and Al_2O_3 for sintering. Similarly, filler rods/wires were made for TIG welding of ZrB_2–SiC based composites. The resulted ZrB_2–SiC based composite is exposed to plasma flame and oxy-propane flame to study its oxidation and thermal protection of carbon fibre reinforced silicon carbide (Cf–SiC).

2 Experimental

PLRS of ZrB_2–SiC composites has been carried out using ZrO_2 and B_4C with two different ratios of 1.6 and 2.0, Si, and sintering additives (Y_2O_3 and Al_2O_3). ZrO_2 powders of size –325# (97.1%) were supplied by Nuclear Fuel Complex, Hyderabad, India. B_4C powders of sinterable grade 1–2 μm size were supplied by China Abrasives, Zing Zhou, China. The details of purity of ZrO_2 and B_4C were reported elsewhere [19,25]. Elemental Si of –325# was supplied by the Metal Powder Company Ltd., Thirumangalam, India. Al_2O_3 of super fine size ($d_{50} \approx 0.7$ μm) obtained from Alcan and submicron-sized Y_2O_3 were used. After studying the initial results, four more modified compositions by decreasing Si and YAG (Y_2O_3+Al_2O_3) contents have been prepared. The initial weight percentage of different powders (ZrO_2, B_4C, Si, Y_2O_3, and Al_2O_3) and designation of respective compositions are given in Table 1.

Table 1 Designation and mechanical properties of different PLRS compositions

	Composition (wt%)					ZrO_2/Si	Measured density (g/cm^3)	Open porosity (%)	VHN at 200 g (GPa)	Flextural strength (MPa)
	ZrO_2	B_4C	Si	Y_2O_3	Al_2O_3					
ZrO_2/B_4C=1.6	44.50	27.83	13.91	6.87	6.87	3.20	4.00	5.28	10.96	—
ZrO_2/B_4C=2.0	52.93	26.46	13.23	3.20	4.16	4.00	4.20	4.90	12.70	117.60
2M1	59.00	29.50	7.37	1.78	2.32	8.00	2.90	22.00	—	—
2M2	62.00	31.00	6.00	0.50	0.50	10.33	4.20	13.00	—	—
2M3	58.67	29.33	10.00	1.00	1.00	5.86	4.15	3.30	15.75	—
2M4	56.00	28.00	14.00	1.00	1.00	4.00	4.10	3.60	13.00	—

The powders and cylindrical alumina balls in weight percentage ratio of 1:1 were taken in polythene bottle and dry mixing of powders on roller mill at 100 rpm was done for 24 h. Green compacts of 60 mm in diameter were made using PVA binder in water solution and uni-axial compaction with a load of 9–10 t. The PLRS was carried out in a graphite resistance heating furnace (Model 1000-3060-FP20, ASTRO, USA). Initially, the furnace was evacuated to 5×10^{-2} Torr vacuum and filled with argon up to a pressure of 1 atm. Heating in vacuum was performed up to a temperature of 1020 ℃ to facilitate de-binding. Honeywell radiation pyrometer Model 939A3 was used to monitor the temperature. 15 ℃/min heating rate was employed. The PLRS experiments were conducted at different temperatures between 1500 and 1680 ℃ in argon atmosphere for 1 h. To avoid total melting of the sample when directly heated to above 1600 ℃, holding for minimum time of 0.5 h at 1550±25 ℃ was employed. After optimising the sintering temperature with 2.0 composite, all other composites reported in Table 1 were sintered at 1680 ℃ in argon atmosphere for 1 h. Compacts of 30 mm in diameter and 10 mm in height were also made by PLRS to study the oxidation at high temperature by exposing to plasma flame of 2700 ℃ and oxy-propane flame of 2300 ℃.

After studying the oxidation behavior by exposing to plasma flame at 2700 ℃, the PLRS 2.0 composite was selected as filler for joining PLRS composites. From the dry mixed powders, thick paste was made using PVA binder in water solution. The paste taken into a medical syringe without fixing needle was extruded to get rods of 7–10 cm in length and ~3 mm in diameter. Green filler extrusions were dried in an oven at 110 ℃ for 1 h. The PLRS was carried out at 1650 ℃ in argon atmosphere for 1 h.

Samples of size 4×5×50 mm long were used for TIG welding of PLRS composites to themselves. The surfaces of samples were ultrasonically cleaned in acetone before joining. The bar samples were placed on a steel table at butt weld gap of ~1 mm. No pre-heating was employed. Manual welding was carried out at a speed of 3 mm/min with 90–120 A welding current. After joining, the argon flow was continued till the joint temperature was less than 800 ℃. Similarly, welding was also performed on the opposite side. TIG welding machine of ESAB make, Model TIG 300A, Kolkata, India, was used.

Bulk density of sintered samples was measured using water displacement method. The sintered samples or joints were cut using diamond cutting wheel or CNC wire cut EDM. The cut pieces were mounted in epoxy and polished using fine diamond (0.25 μm) abrasive to mirror finish. Three-point bending specimens of size 4×5×50 mm were prepared. The flexural strength as per ASTM standard C1161-94 was tested on Instron of model No. 8801 with a span of sample of 40 mm and cross head speed of 0.5 mm/min. The samples of PLRS 2.0 composite were tested at room temperature.

The oxidation behavior was tested by exposing samples of 30 mm in diameter and 10 mm in height to plasma flame at 2700 ℃. A precision optical pyrometer supplied by Pyrometer Instrument Co., Inc., USA, was used to measure the temperature of flame and sample. The samples were exposed continuously for 600 s. After measuring the flame temperature, the sample temperature was measured immediately after withdrawing the flame. Further, rectangular pieces (10 mm × 25 mm × 3 mm) of Cf–SiC composite were exposed to oxy-propane flame of 2300 ℃ in 30 s interval for 20 times with protection of PLRS 2.0 composite and without any protection. The sample of 30 mm in diameter and 10 mm in thickness was cut to make a hemi circular piece to cover the Cf–SiC composite. After every 30 s of flame exposure, the samples were weighed.

The polished cross sections of samples were analyzed for microstructure using an optical microscope and scanning electron microscope (SEM, FEI Quanta 400, Netherlands). The DM H-2, Matsuzawa Seiki, Japan, Vickers micro hardness tester was used with a load of 200 g and a dwell time of 15 s. Phase analysis was carried out with a Philips X-ray diffractometer, Model PW3710, with Cu Kα radiation through Ni filter. Specimens for shear test were extracted from the weld interface region as per ASTM A264 standard. Using a stainless steel fixture in Walte-BaiAg, HTV-1200, universal testing machine, the shear strength of the weld was measured. A cross head speed of 0.1 mm/min was used. Maximum load value divided by the overlap area was calculated to measure the shear strength.

3 Results and discussion

In Fig. 1, the XRD patterns of different PLRS composites are shown and compared with PLS composite [25]. The XRD pattern of 1.6 composite is similar to that of ZrB_2–SiC–B_4C PLS composite with Al_2O_3+Y_2O_3 additions. In 1.6 composite an extra phase of zirconium silicate (ZS) with considerable intensity has been identified. The intensity of ZS phase decreased

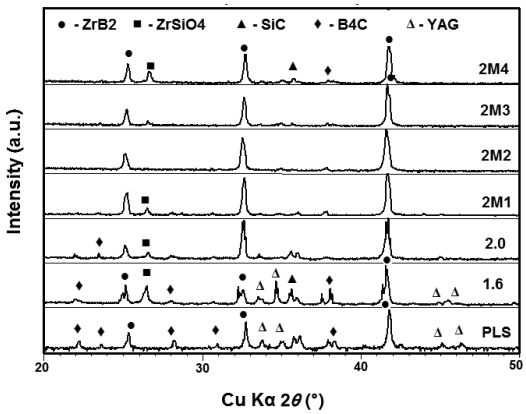

Fig. 1 XRD patterns of PLS [19] and different PLRS composites sintered at 1680 ℃.

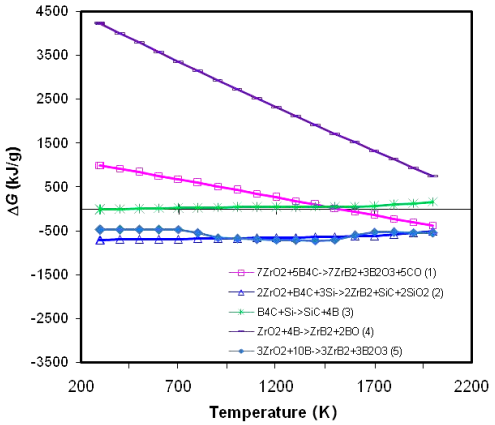

Fig. 2 Gibbs free energy of different reactions as a function of temperature.

with decrease in Si content from ZrO_2/Si = 3.2–4.0 in 2.0 composite. Further decrease in Si content in 2M1 and 2M2 resulted in decrease in intensity or absence of ZS peak in XRD pattern of 2M1 and 2M2 respectively. Similar effect on the intensity of SiC peaks of 2M1 and 2M2 was observed. Since the quantity of Si and Y_2O_3+Al_2O_3 was decreased the densification of the 2M1 and 2M2 composites decreased with increase in porosity (Table 1). Further, increase in the quantity of Si and Al_2O_3+Y_2O_3 in 2M3 and 2M4 caused the reappearance of ZS phase, increase in the intensity of SiC phase, and increase in densification.

The peak at $2\theta = 23.5°$ was identified as B_4C for PLS composite [25]. This peak was absent in the XRD pattern of 1.6 composite. It reappeared in the XRD pattern of 2.0 composite. The grain size and morphology of B_4C affects its XRD pattern. Significant changes in the height and width of diffraction peaks are observed on B_4C synthesized at different temperatures [26]. The relative quantities of three liquid forming materials, *viz.*, Si, Y_2O_3, and Al_2O_3 can affect the grain size, morphology, and volume fraction of excess B_4C.

To obtain a single phase ZrB_2 without impurities like un-reacted ZrO_2, B_4C, and free C, the excess of B_4C in weight percentage ratio of $ZrO_2/B_4C = 2.5$ is required, where the stoichiometric weight ratio in reaction (1) is ~3.0 [19]. In this work, the ratio of $ZrO_2/B_4C = 1.6$ and 2.0 was chosen to have excess B_4C to aid in sintering of the composite.

$$7ZrO_2 + 5B_4C \rightarrow 7ZrB_2 + 3B_2O_3 + 5CO \quad (1)$$

$$\Delta G^\circ_{298} = +1000.0 \text{ kJ/g}, \ \Delta H^\circ_{298} = +1239.2 \text{ kJ/g}$$

$$2ZrO_2 + B_4C + 3Si \rightarrow 2ZrB_2 + SiC + 2SiO_2 \quad (2)$$

$$\Delta G^\circ_{298} = -700.1 \text{ kJ/g}, \ \Delta H^\circ_{298} = -710.1 \text{ kJ/g}, \ T_{ad} \approx 1175 \text{ K}$$

From thermodynamic calculations in Fig. 2, reaction (1) is feasible at and above a temperature of 1250 ℃ (1523 K). When Si is also present, reaction (2) is more feasible with $T_{ad} \approx 1175$ K. But it is an ordinary reaction and cannot progress in self-sustaining manner. The feasibility of an SHS reaction can be determined using the adiabatic combustion temperature (T_{ad}), the maximum temperature that can be attained for a given reaction system. If the adiabatic temperature $T_{ad} \geqslant$ 1800 K, the SHS reaction is possible according to Merzhanov criterion [27]. Since this reaction does not satisfy the Merzhanov criterion, it will not progress in self-sustaining manner. Even by rapid heating of a compact of ZrO_2+B_4C+Si by suddenly introducing into the furnace, formation of ZrB_2 and SiC was observed at and above a temperature of 1300 ℃ only [19].

Reaction (3) is feasible at low temperature of 298–300 K only. But Si reacts with C in B_4C at about 1300 ℃ to form SiC. The boron released from B_4C reacts with ZrO_2 to form ZrB_2 according to reaction (4). High temperature of about 2500 K is required for completion of the reaction (4). Braton and Nicholls [28] used the reaction (4) and obtained ZrB_2+BO gas at 1150 ℃. Peshev and Bliznakov [12] reported that a temperature of 1600 ℃ was needed for the completion of reaction of ZrO_2 with boron. Ran *et al.* [29] studied the borothermal reduction of nanometric ZrO_2 powders to synthesize submicrometer-sized ZrB_2 powders in vacuum. ZrO_2 was completely converted into ZrB_2 when thermally treated at a temperature of 1000 ℃ for 2 h in a vacuum.

$$B_4C + Si \rightarrow SiC + 4B \quad (3)$$

$$\Delta G^\circ_{298} = -3.6 \text{ kJ/g}, \ \Delta H^\circ_{298} = -25.1 \text{ kJ/g}, \ T_{ad} \approx 323 \text{ K}$$

$$ZrO_2 + 4B \rightarrow ZrB_2 + 2BO \quad (4)$$

$$\Delta G^{\circ}_{298} = +4239\ \text{kJ/g},\ \Delta H^{\circ}_{298} = +4900\ \text{kJ/g}$$

$$3ZrO_2 + 10B \rightarrow 3ZrB_2 + 2B_2O_3 \quad (5)$$

$$\Delta G^{\circ}_{298} = -462.9\ \text{kJ/g}, \Delta H^{\circ}_{298} = -458.9\ \text{kJ/g},\ T_{ad} \approx 782.6\ \text{K}$$

Reaction (5) is feasible at all temperatures (Fig. 2). Recently Guo *et al.* [30] reported the formation of fine ZrB_2 through borothermal reduction of coarse ZrO_2 (reaction (5)). Thus the addition of silicon is found to favour the reactions (2)–(5).

Si and Y_2O_3+Al_2O_3 are main constituents to form liquid glass phase (YAG) at high temperature. From Table 1, it is clear that Y_2O_3+Al_2O_3 has also little effect on formation of ZS phase in Fig. 1. Even after decreasing the Y_2O_3+Al_2O_3 content in 2M3 and 2M4 with increase in Si content, the ZS phase reappeared in 2M4. The ratio of ZrO_2/Si is crucial in the formation of ZS phase. The stoichiometric ratio of ZrO_2/Si according to reaction (2) is 2.93. ZS phase is observed with Si as low as ZrO_2/Si = 8 in 2M1. According to reaction (2), out of 3 moles of Si, 2 moles are consumed to form SiO_2. At high temperature, SiO_2 escapes from the system as SiO. Since the reactant powders are compacted and sintering mechanism starts at lower temperature in presence of Y_2O_3+Al_2O_3, the entrapped SiO_2 reacts with residual ZrO_2 to form a stabilized ZS phase. The formation of ZS phase was not reported when the reactants (ZrO_2, B_4C, and Si) are in the form of loose powders or compacts [19]. At sintering temperature as low as 1500 ℃, slight shrinkage of PLRS 2.0 sample due to sintering has been observed (Fig. 3). The appearance of sintered samples in Fig. 3 confirmed that *in situ* formed SiO_2 in reaction (2) could not escape due to densification and reacted with ZrO_2 to form ZS phase.

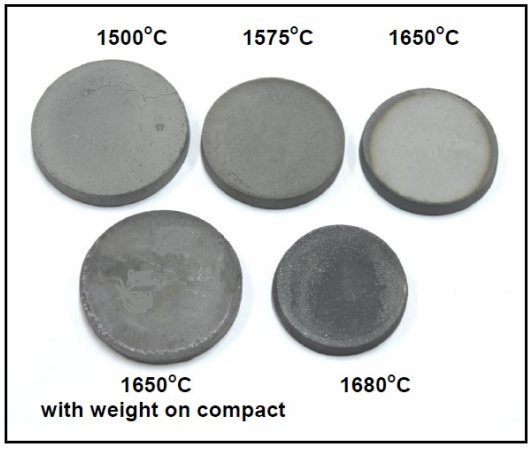

Fig. 3 Appearance of 2.0 composite after PLRS at different temperatures.

Due to the formation of large quantity of liquid phase, heating rapidly to above 1600 ℃ can lead to melting of the sample and reaction with graphite crucible. To avoid total melting of the sample when directly heated to above 1600 ℃, holding for minimum time of 0.5 h at 1550±25 ℃ was employed. The appearance of compacts of 2.0 composite of 60 mm in diameter after PLRS at different temperatures is shown in Fig. 3. Rapid heating to high temperature of 1600 ℃ has been found to cause total melting or warpage of the sample to form concave/convex shape. To avoid this uneven shrinkage, cylindrical graphite black can be placed on the compact. During synthesis, the yield of ZrB_2 from ZrO_2+B_4C is around 65% of the weight of total reactants [25]. Similarly, the volumetric shrinkage during PLS of ZrB_2–SiC–B_4C composite is 20%–30%. Since synthesis and sintering are occurring in a single step, the total shrinkage will be about 40% in PLRS. So the rate of heating and maximum sintering temperature play major role in retaining the shape of the final component.

The SEM and BSE images of 1.6 and 2.0 composites sintered at 1680 ℃ are shown in Fig. 4. Apart from ZrB_2 and SiC, YAG and ZS phases were identified in 1.6 composite (Fig. 4(b)). Similarly, ZrB_2, SiC, and YAG phases were identified in 2.0 composite (Fig. 4(d)). There is a large difference in the morphology of ZrB_2 from 1.6 to 2.0 composite. ZrB_2 grains are large (≈ 50 μm) and elongated in 2.0 composite and spherical or isometrical in 1.6 composite. It appears that Si, Y_2O_3, and Al_2O_3 are three liquid forming constituents controlling the morphology and size of ZrB_2. The decrease in the total Y_2O_3+Al_2O_3 content from 13.74 to 7.36 wt% facilitated the growth of elongated grains in

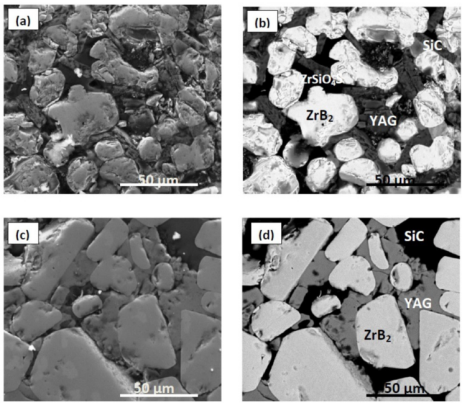

Fig. 4 SEM images after PLRS at 1680 ℃: (a) 1.6 composite and (c) 2.0 composite, and corresponding BSE images: (b) 1.6 composite and (d) 2.0 composite.

2.0 composite. The typical morphologies of 2M1 and 2M2 are shown in Figs. 5(a) and 5(b). The grain size of ZrB_2 was found to decrease with decrease in total $Si+Y_2O_3+Al_2O_3$ content from 11.47 in 2M1 to 7.0 wt% in 2M2 (Table 1). Further, increase in total $Si+Y_2O_3+Al_2O_3$ content to 12.00 wt% resulted in increase of the ZrB_2 grain size in 2M3 (Fig. 5(c)). The morphology of 2M4 (Fig. 5(d)) is similar to that of 2.0 composite (Fig. 4(d)). Since the ratio of ZrO_2/Si is 4 in both 2.0 and 2M4, the small grain size in 2M4 can be attributed to decrease in $Y_2O_3+Al_2O_3$ content from 7.36 in 2.0 composite to 2.0 wt% in 2M4 composite (Table 1). Though the $Y_2O_3+Al_2O_3$ content is similar in 2M3 and 2M4, the increase in Si from 12.00 in 2M3 to 16.00 wt% in 2M4 resulted in increase in grain size of ZrB_2.

The measured bulk densities of different PLRS composites varied from 2.90 to 4.20 $g \cdot cm^{-3}$, for 2M1 to 2.0 composites (Table 1). There is large difference in densities from calculated values to measured values. This could be due single-step synthesis and sintering. Loss of oxide vapors of all constituents of reactants and products during synthesis can lead to considerable weight loss (> 30%) for different composites. Under free flow of argon during liquid phase sintering, loss of gaseous species is possible. Since there are many reactants (Si, SiO_2, ZrO_2, and B_2O_3), additives (Y_2O_3 and Al_2O_3), and product phases (ZrB_2, SiC, and B_4C), the reaction among them during synthesis and sintering is unknown. The densification mechanism may be controlled by dissolution–precipitation or evaporation–condensation [31]. During liquid phase sintering of YAG/ZrB_2, a sintering temperature of 1600 ℃ is a critical temperature to form molten YAG and to achieve a full density [32]. Since the values of true densities of the sintered composites are not known, the comparison of the measured bulk densities indicates the trend of increasing or decreasing [33]. The open porosity varied from 3.3% to 22%. Since synthesis and sintering are advancing simultaneously in single-step process, the quantities of Si and YAG play very important role on densification, grain size, and morphology of ZrB_2 and SiC.

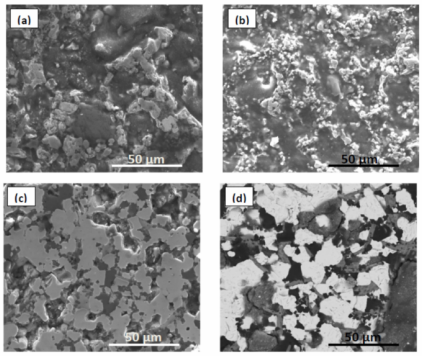

Fig. 5 SEM images of (a) 2M1, (b) 2M2, (c) 2M3, and (d) BSE image of 2M4 composites PLRS at 1680 ℃.

Vickers hardness number (VHN) for all PLRS samples varied from point to point due to the presence of soft (ZS and YAG) and hard (ZrB_2 and SiC) phases. A large number of readings were taken and average values were calculated. The VHN increased from 10.96 GPa for 1.6 composite to 12.70 GPa for 2.0 composite. Similarly, VHN decreased from 15.75 GPa for 2M3 composite to 13.00 GPa for 2M4 composite. The hardness values are in agreement with phases identified in XRD patterns of PLRS composites (Fig. 1). Considering the density, porosity, and hardness, the 2.0 composite was selected for further detailed studies of flextural strength, high temperature oxidation resistance, and weld ability. With a flextural strength of 117.60 MPa, the 2.0 composite is comparable with PLS ZrB_2–SiC–B_4C composite [25].

Further, the PLRS 2.0 was studied for high temperature oxidation resistance by exposing to plasma flame at 2700 ℃ and compared with PLS ZrB_2–SiC–B_4C composite (Fig. 6). Both PLS and PLRS 2.0 samples exhibited dimensional stability and resistance to thermal shock upon exposure to plasma flame (2700 ℃) for 600 s. Weight gain of 11.67 mg/cm^2 for PLS ZrB_2–SiC–B_4C composite (Fig. 6(b)) and

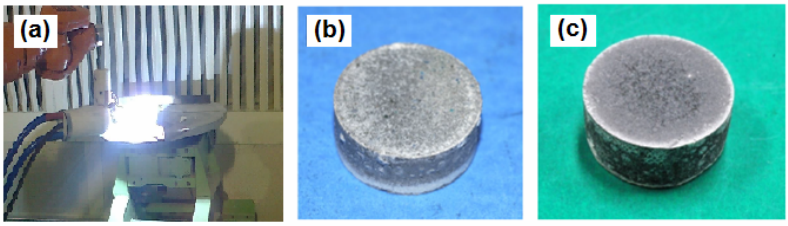

Fig. 6 (a) Sintered sample of 30 mm in diameter being exposed to plasma flame at 2700 ℃. Appearance of samples after 10 min exposure: (b) PLS ZrB_2–SiC–B_4C composite, weight gain +11.67 mg/cm^2 and (c) PLRS 2.0 composite, weight gain +12.75 mg/cm^2.

12.75 mg/cm^2 for PLRS 2.0 composite (Fig. 6(c)) was recorded. Monolithic ZrB_2 oxidizes to form ZrO_2 and B_2O_3 liquid at low temperature of the order of 450 ℃. In the case of ZrB_2–SiC composite, the silicon and boron in the composite are oxidized at elevated temperatures, to form a protective borosilicate glass layer.

$$2ZrB_2(s) + 5O_2(g) \rightarrow 2ZrO_2(s) + 2B_2O_3(l) \quad (6)$$

$$SiC(s) + 3/2O_2 \rightarrow SiO_2(l) + CO(g) \quad (7)$$

But above 1400 ℃, the rate of volatilization of B_2O_3 is higher than the rate of production of B_2O_3. The resultant increase in weight due to the formation of ZrO_2 is greater than the reduction in weight due to the evaporation of B_2O_3. Secondary, ZrO_2 precipitates on the external surface of the oxide scale. So, the oxide scale is a multi-phase layer with its composition, physical properties (like viscosity), and relative amount of phases changing with the temperature. Weight gain measurement does not offer good support to explain any oxidation mechanism because oxidation and vaporization processes are advancing simultaneously. Preliminary comparison of oxidation behavior of different samples can be made. PLS ZrB_2–SiC–B_4C composite after exposing to plasma flame of 2700 ℃ for 600 s recorded a weight gain of 11.67 mg/cm^2. With a recorded weight gain of 12.75 mg/cm^2, the PLRS 2.0 composite is comparable in high temperature oxidation resistance with PLS ZrB_2–SiC–B_4C composite.

The BSE image of oxide layer of PLRS 2.0 composite after 10 min exposure to plasma flame at 2700 ℃ is shown in Fig. 7(a). The corresponding XRD pattern of PLRS 2.0 composite exposed to plasma flame is shown in Fig. 8(a). Formation of yttria stabilized zirconia (YSZ), silica, and YAG phases on the oxidized surface was observed. ZrO_2 alone cannot adhere to ZrB_2 at high temperatures and undergo cracking. The difference in coefficient of thermal expansion between oxide scale and unaltered ZrB_2 matrix causes weak bonding and spalling [34]. In PLRS 2.0 composite, the YSZ precipitates from BSZ glass and remains embedded in complex YAG layer. Continuous and compact ZrO_2 embedded in YAG that adhere to parent composite protect it from further oxidation by preventing direct exposure of the ZrB_2–SiC composite to air. The EDS of parent composite of PLRS 2.0 after 10 min exposure to plasma flame at 2700 ℃ (Fig. 8(b)) revealed the retention of unaltered phases: bright phase of ZrB_2, grey phase of SiC, and dark phase of complex YAG.

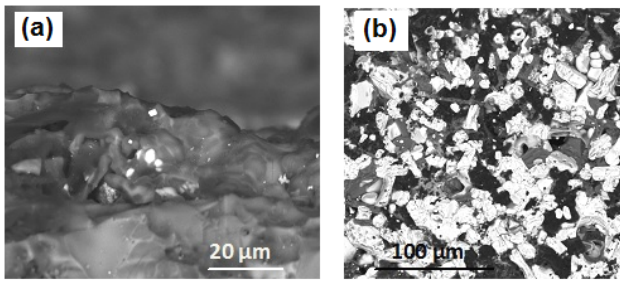

Fig. 7 BSE images of (a) oxide layer and (b) parent composite of PLRS 2.0 after 10 min exposure to plasma flame at 2700 ℃.

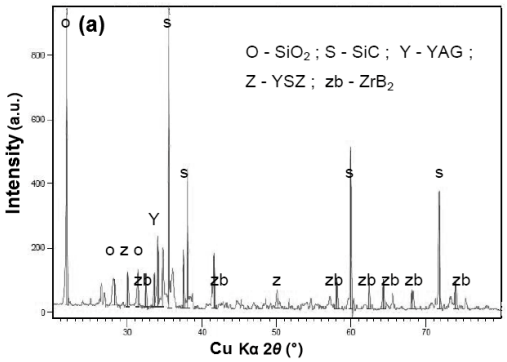

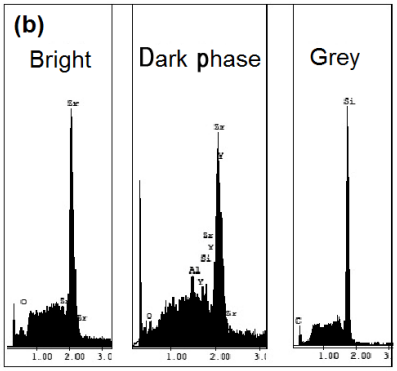

Fig. 8 (a) XRD pattern of oxide layer and (b) EDS of parent composite of PLRS 2.0 after 10 min exposure to plasma flame at 2700 ℃.

Since ZrB_2 is electrically conductive, arc fusion welding is possible. Due to high melting point during fusion welding of ZrB_2 based composites, oxidation and formation of porosity in the melt fusion zone occur. When melt pool is solidified with high volume change, formation of voids or porosity at boundary of parent material and fusion zone is expected. Owing to the properties of ZrB_2: high thermal expansion coefficient (5.9×10^{-6} K^{-1}), high Young's modulus (489 GPa), and low fracture toughness (3.5 MPa·m^{-2}), rapid heating or cooling results in large thermal gradient and thermal shock failure through crack initiation [35]. Earlier

efforts on fusion welding by pre heating and controlled cooling under protective atmosphere also lead to thermal shock failure or porosity at the weld interfaces of TiB_2–20 vol% TiC and ZrB_2–20 vol% ZrC composites [36,37].

Using a suitable filler material, formation of cracks, pores, and voids can be avoided [38]. When arc is struck, filler material melts and forms a liquid pool to fill the gap between the weld surfaces to be joined. The flow of molten filler into weld gap is similar to metal casting into a mold. Cracks and pores that could form due to shrinkage during the solidification of filler can be avoided by controlling the welding speed or flow of the molten filler into weld gap. The filler material should be chosen with good flow ability and oxidation resistance to flow freely into the weld gap. After studying the oxidation behavior by exposing to plasma flame at 2700 ℃, the 2.0 composite was selected as filler for joining PLRS composites.

Flextural test samples of size 4×5×50 mm of PLRS 2.0 composite were used for TIG welding. The weld is very clean and free from cracks and appeared similar to that of metal weld. Oxidation of neither parent material nor filler material was observed. No cracks and pores on either side of the joint interface were observed after welding with filler (Fig. 9(a)). Examination of the cross section of the weld revealed that the joint interface between the parent material and filler material was very clean and coherent (Fig. 9(b)). Typical dendrite structure of solidified filler material can be seen. Tungsten impurity (bright phase) picked up from tungsten electrode was identified in Fig. 9(c). The grey phase ZrB_2 and dark phase SiC were identified through EDS analysis. During shear testing in steel fixture the PLRS 2.0 welds failed in weld zone. SEM image of the morphology of fracture surface confirmed the cleavage/brittle mode fracture (Fig. 9(d)). Shear strength of the weld was 63.5 MPa. This is lower than the three-point bend flextural strength of 117.6 MPa for PLRS 2.0 composite. The shear strength of the weld was about 55% of the flexural strength of the parent composite.

For TPS application, high mechanical performance is not required. High oxidation resistance and thermal shock resistance are the main material requirements [24]. The peak thermal stress of UHTC wing leading edge under re-entry heating conditions is predicted to be 80 MPa [21]. It is well below the strength of PLRS 2.0 composite. The composite is shown to be oxidation resistant, thermal shock resistant, and easily

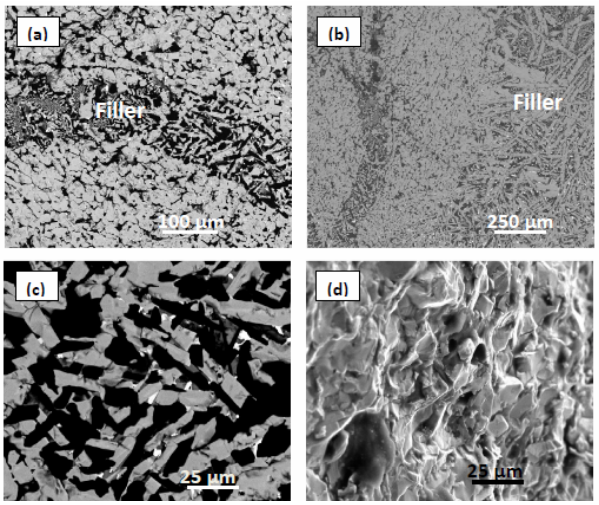

Fig. 9 (a) and (b) BSE images of cross section of welded PLRS 2.0 composite. (c) Filler area at higher magnification: dark phase SiC, grey phase ZrB_2, and bright phase tungsten. (d) SEM image of fracture surface after shear testing of the welded sample.

formable/weldable. The possibility of using the PLRS ZrB_2–SiC based composite for thermal protection of Cf–SiC composite is examined. Rectangular pieces (10 mm × 25 mm × 3 mm) of Cf–SiC composite are exposed to oxy-propane flame of 2300 ℃ in 30 s interval for 20 times with protection of PLRS 2.0 composite and without any protection. After every 30 s of flame exposure, the samples were weighed. Schematic diagram of the arrangement of Cf–SiC composite specimen for exposure to oxy-propane flame is shown in Figs. 10(a)–10(e). Cf–SiC composite is placed on a graphite block and covered with PLRS 2.0 composite. The sintered PLRS 2.0 composite of 30 mm in diameter was cut to make a shape similar to leading edge and covered the Cf–SiC composite. Without protection the Cf–SiC composite is placed on hemi circular pieces of PLS composite and directly exposed to flame (Fig. 10(e)). The temperature of PLRS 2.0 and Cf–SiC composites was measured immediately after withdraw of the flame. The appearance of specimens during exposure, during cooling, and after exposure for total 600 s is shown in Fig. 10.

With protection from PLRS 2.0 composite, a weight gain of 0.064% was recorded for Cf–SiC composite. The bare Cf–SiC composite gained a weight of 6.66% after a total of 600 s of exposure to oxy-propane flame. This result clearly shows that the PLRS ZrB_2–SiC based composite is capable of providing thermal protection for Cf–SiC composite at high temperatures. The present results revealed the possibility of synthesis and

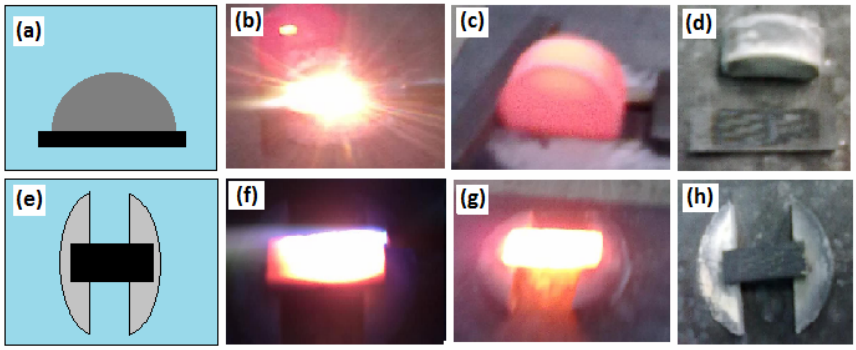

Fig. 10 Arrangement of Cf–SiC composite specimen (black) for exposure to oxy-propane flame of 2300 ℃: (a) with protection of PLRS 2.0 composite, (b) during exposure to flame, (c) during cooling, and (d) after exposure for total 600 s. (e) Cf–SiC composite without protection, (f) during exposure to flame, (g) immediately after withdrawn of the flame, and (h) after exposure for total 600 s.

sintering of ZrB_2–SiC based composites in a single step by PLRS at relatively low temperatures between 1550 and 1680 ℃ using ZrO_2, B_4C, and Si as raw materials. The PLRS ZrB_2–SiC based composites are shown to be oxidation resistant, thermal shock resistant, easily formable/weldable, and useful for thermal protection application.

4 Conclusions

Synthesis and sintering of ZrB_2–SiC based composites have been carried out in a single step by pressureless reaction sintering (PLRS) using ZrO_2+B_4C+Si for synthesis and Y_2O_3+Al_2O_3 for sintering. The effect of ratios of ZrO_2/B_4C, ZrO_2/Si, and sintering additives (Y_2O_3 and Al_2O_3), was studied by sintering at different temperatures between 1500 and 1680 ℃ in argon atmosphere. ZrB_2, SiC, and YAG phases were identified in the sintered compacts. The mechanical properties of the PLRS composite are comparable with those properties obtained for pressureless sintered (PLS) composites. Filler material was also prepared by PLRS for tungsten inert gas welding of the ZrB_2–SiC based PLRS composites. The ZrB_2–SiC based PLRS composites exhibited high resistance to oxidation and thermal shock upon exposure to plasma flame at 2700 ℃ for 600 s. The composites were found suitable for thermal protection of Cf–SiC composites.

Acknowledgements

Authors acknowledge the financial support from the Defence Research and Development Organization, Ministry of Defence, Government of India, New Delhi, India, in order to carry out the present study under project DMR-295. They are grateful to the Director of DMRL, Hyderabad, for his constant encouragement. The authors acknowledge the support from various characterization groups of DMRL.

References

[1] Upadhya K, Yang JM, Hoffmann WP. Materials for ultrahigh temperature structural applications. *Am Ceram Soc Bull* 1997, **76**: 51–56.

[2] Fahrenholtz WG, Hilmas GE, Talmy IG, *et al*. Refractory diborides of zirconium and hafnium. *J Am Ceram Soc* 2007, **90**: 1347–1364.

[3] Mroz C. Zirconium diboride. *Am Ceram Soc Bull* 1994, **73**: 141–142.

[4] Balak Z, Shahedi Asl M, Azizieh M, *et al.* Effect of different additives and open porosity on fracture toughness of ZrB_2–SiC-based composites prepared by SPS. *Ceram Int* 2017, **43**: 2209–2220.

[5] Balak Z, Azizieh M, Kafashan H, *et al.* Optimization of effective parameters on thermal shock resistance of ZrB_2–SiC-based composites prepared by SPS: Using Taguchi design. *Mater Chem Phys* 2017, **196**: 333–340.

[6] Shahedi Asl M, Golmohammadi F, Kakroudi MG, *et al.* Synergetic effects of SiC and C_{sf} in ZrB_2-based ceramic composites. Part I: Densification behavior. *Ceram Int* 2016, **42**: 4498–4506.

[7] Shahedi Asl M, Kakroudi MG, Farahbakhsh I, *et al.* Synergetic effects of SiC and C_{sf} in ZrB_2-based ceramic composites. Part II: Grain growth. *Ceram Int* 2016, **42**: 18612–18619.

[8] Farahbakhsh I, Ahmadi Z, Shahedi Asl M. Densification, microstructure and mechanical properties of hot pressed ZrB_2–SiC ceramic doped with nano-sized carbon black. *Ceram Int* 2017, **43**: 8411–8417.

[9] Ahmadi Z, Nayebi B, Shahedi Asl M, *et al.* Fractographical characterization of hot pressed and pressureless sintered

AlN-doped ZrB_2–SiC composites. *Mater Charact* 2015, **110**: 77–85.
[10] Zhao H, He Y, Jin Z. Preparation of zirconium boride powder. *J Am Ceram Soc* 1995, **78**: 2534–2536.
[11] Guo W-M, Zhang G-J. Reaction processes and characterization of ZrB_2 powder prepared by boro/carbothermal reduction of ZrO_2 in vacuum. *J Am Ceram Soc* 2009, **92**: 264–267.
[12] Peshev P, Bliznakov G. On the borothermic preparation of titanium, zirconium and hafnium borides. *J Less Common Met* 1968, **14**: 23–32.
[13] Chen L, Gu Y, Yang Z, *et al.* Preparation and some properties of nanocrystalline ZrB_2 powders. *Scripta Mater* 2004, **50**: 959–961.
[14] Radev DD, Marinov M. Properties of titanium and zirconium diborides obtained by self-propagated high-temperature synthesis. *J Alloys Compd* 1996, **244**: 48–51.
[15] Zou J, Zhang G-J, Zhang H, *et al*. Improving high temperature properties of hot pressed ZrB_2–20 vol% SiC ceramic using high purity powders. *Ceram Int* 2013, **39**: 871–876.
[16] Qiu H-Y, Guo W-M, Zou J, *et al*. ZrB_2 powders prepared by boro/carbothermal reduction ZrO_2: The effects of carbon source and reaction atmosphere. *Powder Technol* 2012, **217**: 462–466.
[17] Yuan H, Li J, Shen Q, *et al*. Preparation and thermal conductivity characterization of ZrB_2 porous ceramics fabricated by spark plasma sintering. *Int J Refract Met H* 2013, **36**: 225–231.
[18] Yuan H, Li J, Shen Q, *et al*. *In situ* synthesis and sintering of ZrB_2 porous ceramics fabricated by spark plasma sintering-reactive synthesis (SPS-RS) method. *Int J Refract Met H* 2012, **34**: 3–7.
[19] Krishnaro RV, Alam MZ, Das DK, *et al*. Synthesis of ZrB_2–SiC composite powder in air furnace. *Ceram Int* 2014, **40**: 15647–15653.
[20] Krishnarao RV, Sankarasubrahmanian R. Thermite assisted synthesis of ZrB_2 and ZrB_2–SiC through B_4C reduction of ZrO_2 and $ZrSiO_4$ in air. *J Adv Ceram* 2017, **6**: 139–148.
[21] Johnson SM. Ultra high temperature ceramics UHTCs. NASA Technical Report. 2015. Available at https://ntrs.nasa.gov/archive/nasa/casi.ntrs.nasa.gov/20150022996.pdf.
[22] Orcutt M. Heat resistant ceramic parts are now 3-D printable. Available at http://www.technologyreview.com/news/545086/heat-resistant-ceramic-parts-are-now-3-D-printable/.
[23] Eckel ZC, Zhou C, Martin JH, *et al.* Additive manufacturing of polymer-derived ceramics. *Science* 2016, **351**: 58–62.
[24] Padovano E. Ceramic multilayer based on ZrB_2/SiC system for aerospace applications. Ph.D. Thesis. Politecnico di Torino, 2015.
[25] Krishnaro RV, Alam MZ, Das DK, *et al*. Pressureless sintering of (ZrB_2–SiC–B_4C) composites with (Y_2O_3 + Al_2O_3) additions. *Int J Refract Met H* 2015, **52**: 55–65.
[26] Anselmi-Tamburini U, Ohyanagi M, Munir ZA. Modelling studies of the effect of twins on the X-ray diffraction patterns of boron carbide. *Chem Mater* 2004, **16**: 4347–4351.
[27] Merzhanov AG. Self-propagating high temperature synthesis: Twenty years of research and findings. In: *Combustion and Plasma Synthesis of High Temperature Materials*. Munir Z, Holt IB, Eds. New York: VCH, 1990: 1–53.
[28] Barton L, Nicholls D. The hydrogenation of boron monoxide to diborane and the reactions of boron and boron carbide with titanium and zirconium dioxides. *J Inorg Nucl Chem* 1996, **28**: 1367–1372.
[29] Ran S, van der Biest O, Vleugel J. ZrB_2 powders synthesis by borothermal reduction. *J Am Ceram Soc* 2010, **93**: 1586–1590.
[30] Guo WM, Tan DW, Zhang ZL, *et al.* Synthesis of fine ZrB_2 powders by new borothermal reduction of coarse ZrO_2 powders. *Ceram Int* 2016, **42**: 15087–15090.
[31] Zhang X, Li X, Hana J, *et al.* Effects of Y_2O_3 on microstructure and mechanical properties of ZrB_2–SiC ceramics. *J Alloys Compd* 2008, **465**: 506–511.
[32] Song J-G, Li J-G, Song J-R, *et al.* Preparation of high-density YAG/ZrB_2 multi-phase ceramics by spark plasma sintering. *J Ceram Process Res* 2007, **8**: 356–358.
[33] Fahrenholtz WG, Neuman EW, Brown-Shaklee H-J, *et al*. Superhard boride-carbide particulate composites. *J Am Ceram Soc* 2010, **93**: 3580–3583.
[34] Zhang X, Hu P, Han J, *et al*. Ablation behavior of ZrB_2–SiC ultra high temperature ceramics under simulated atmospheric re-entry conditions. *Comp Sci Tech* 2008, **68**: 1718–1726.
[35] Zimmermann JW, Hilmas GE, Fahrenholtz WG. Thermal shock resistance of ZrB_2 and ZrB_2–30% SiC. *Mater Chem Phys* 2008, **112**: 140–145.
[36] King DS, Hilmas GE, Fahrenholtz WG. Plasma arc welding of TiB_2–20 vol% TiC. *J Am Ceram Soc* 2014, **97**: 56–59.
[37] King DS, Hilmas GE, Fahrenholtz WG. Plasma arc welding of ZrB_2–20 vol% ZrC ceramics. *J Eur Ceram Soc* 2014, **34**: 3549–3557.
[38] Krishnaro RV, Reddy GM. Gas tungsten arc welding of (ZrB_2–SiC) based ultra high temperature ceramic composites. *Defence Tech* 2015, **11**: 188–196.